Applied Surface Science 354 (2015) 229–234

Contents lists available at ScienceDirect

Applied Surface Science

journal homepage: www.elsevier.com/locate/apsusc

Tight-binding parameters of graphite determined with angle-resolved photoemission spectra

Cheng-Maw Cheng[a,*], Chia-Jen Hsu[b], Jian-Lun Peng[b], Ching-Hung Chen[a], Jih-Young Yuh[a], Ku-Ding Tsuei[a,b]

[a] National Synchrotron Radiation Research Center, 101 Hsin-Ann Road, Hsinchu 30076, Taiwan
[b] Department of Physics, National Tsing Hua University, 101 Sec. 2, Kuang-Fu Road, Hsinchu 30013, Taiwan

ARTICLE INFO

Article history:
Received 8 October 2014
Received in revised form
17 December 2014
Accepted 18 December 2014
Available online 7 January 2015

Keywords:
ARPES
Graphite
The tight-binding method
SWMcC model
Band structure

ABSTRACT

An exfoliated Kish graphite sample on a heavily *n*-doped Si substrate covered with native oxide was prepared with a conventional micromechanical cleavage method. From angle-resolved photoemission spectra (ARPES), we measured the band structure of graphite over photon energies from 28 eV to 116 eV. The inner potential V_0 = 17.25 eV is determined with a period from the band dispersion in the *KH* direction. A set of parameters in the tight-binding method and the SWMcC model for graphite is extracted from the fitted results. A comparison of constant-energy mapping results at large binding energy indicates the reliability of the tight-binding parameters extracted from the ARPES results.

1. Introduction

Graphite comprises weakly coupled layers of carbon atoms with a honeycomb structure in two-dimensional sheets. Graphite is a semi-metal because the charge carriers occupy small regions along the edges of the Brillouin zone. For an understanding of the electronic structure of graphite, the tight-binding approach provides direct insight into the interactions between individual carbon atoms. Wallace proposed the first tight-binding model for graphite [1]; soon after, the band structure of graphite was calculated with perturbation methods by Slonzewski and Weiss, and McClure [2,3]. Seven parameters that define the interaction energy of various carbon atoms in graphite lattices were introduced and are referred to as the SWMcC model [4–6]. This model described successfully the band structure of graphite; its seven parameters were evaluated in many experiments, such as the de Haas–van Alphen effect [7–9], SdH oscillation [10–12], infrared spectra [13–16], transport properties [17], high-field magnetoreflectance [18] and angle-resolved photoemission spectra [19,20]. In that SWMcC model, the content of the trigonal warping effect indicated by the value of γ_3 is insensitive to the shape of the Fermi surface, but in many experiments the parameters of the SWMcC model are extracted from the behavior of electron and hole carriers at the Fermi surface, which creates an uncertainty of the determined γ_3 value. In contrast, the trigonal warping effect can affect strongly the shape of contours of constant energy in the region of large binding energy. Angle-resolved photoemission spectra (ARPES) provide a general tool to probe the band structure of solids. In this work, we recorded, at high resolution, ARPES of Kish graphite on a heavily *n*-doped Si substrate over an energy range 28–116 eV. The parameters of the SWMcC model are extracted from the band mapping results. With the tight-binding method we simulated the constant mapping contours in satisfactory agreement with experimental results.

2. Methods

With a conventional micromechanical cleavage method we prepared exfoliated Kish graphite samples on a heavily *n*-doped Si substrate covered with native oxide. Because the spot size of the synchrotron beam can be larger than the size of exfoliated graphite, the advantage of a heavily *n*-doped Si substrate is the presence of a thin native oxide layer that insures negligible charging effects during ARPES measurements and provides a featureless background below 4 eV of the Fermi level. The preparation of an exfoliated Kish sample *ex situ* involved annealing at 500 °C in a UHV environment for 12 h before ARPES measurements. The ARPES experiment

* Corresponding author. Tel.: +886 35780281x6423; fax: +886 35783813.
E-mail address: makalu@nsrrc.org.tw (C.-M. Cheng).

http://dx.doi.org/10.1016/j.apsusc.2014.12.124
0169-4332/

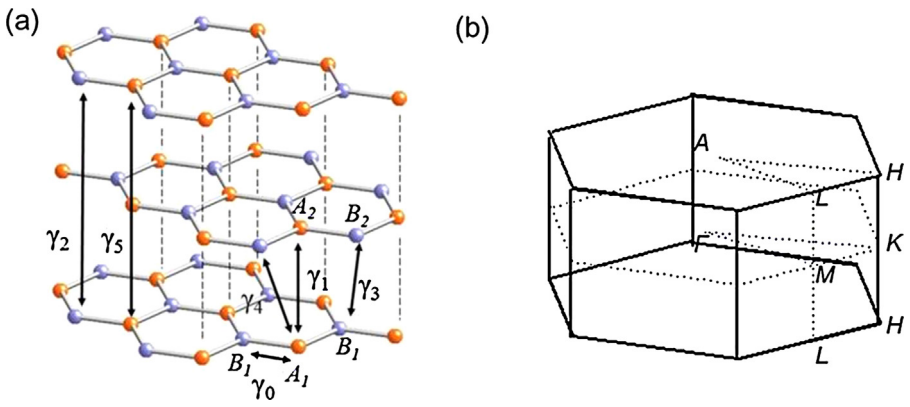

Fig. 1. (a) Crystal structure of graphite; the correspondence denotes the relation between the interactions of individual carbon atoms and the tight-binding parameters γ_i. (b) The Brillouin zone of graphite with the high symmetry points.

was performed at National Synchrotron Radiation Research Center (NSRRC) in Taiwan at beamline BL21B1. The photoemission spectra were collected in an UHV chamber equipped with a hemispherical analyzer (Scienta R4000) at 45 K and base pressure 5×10^{-11} Torr. The total energy resolution is better than 30 meV; the angular resolution is 0.2° over the entire range of photon energy.

3. Tight-binding calculations of graphite

The form of graphite comprises many coupled graphene sheets with Bernal or AB stacking order. A graphene sheet comprises carbon atoms in two sets in a single layer with a honeycomb structure. Two carbon atoms with atoms of basis A and B form a hexagonal structure with a periodic unit cell. A Bernal stacking order has two coupled graphene layers with inequivalent sites A_1 and B_1 on the lower sheets and A_2 and B_2 on the upper sheets. Fig. 1(a) displays the crystal structure of graphite; lattice vectors are described as $\vec{a}_1 = a_0(1/2, \sqrt{3}/2, 0)$, $\vec{a}_2 = a_0(-1/2, \sqrt{3}/2, 0)$ and $\vec{a}_3 = (0, 0, 2c_0)$ in which $a_0 = 2.46$ Å is the lattice parameter and $c_0 = 3.35$ Å is the distance between two adjacent graphene sheets. To understand the electronic structure of graphite, the tight-binding method gives direct insight to sketch its energy band. The tight-binding Hamiltonian of graphite is expressed as [20,21].

$$H\left(\vec{k}\right) = \begin{pmatrix} E_0 + \Delta + \Upsilon_5(\Gamma^2 - 2) & \gamma_0 f(\vec{k}) & \gamma_1 \Gamma & \gamma_4 \Gamma f^*\left(\vec{k}\right) \\ \gamma_0 f^*(\vec{k}) & E_0 + \gamma_2(\Gamma^2 - 2) & \gamma_4 \Gamma f^*\left(\vec{k}\right) & \gamma_3 \Gamma f(\vec{k}) \\ \gamma_1 \Gamma & \gamma_4 \Gamma f(\vec{k}) & E_0 + \Delta + \gamma_5(\Gamma^2 - 2) & \gamma_0 f^*(\vec{k}) \\ \gamma_4 \Gamma f(\vec{k}) & \gamma_3 \Gamma f^*(\vec{k}) & \gamma_0 f\left(\vec{k}\right) & E_0 + \gamma_2(\Gamma^2 - 2) \end{pmatrix}$$

in which the tight-binding hopping parameters γ_0, γ_1, γ_2, γ_3, γ_4, γ_5, Δ are described in Fig. 1(b); $f\left(\vec{k}\right) = \exp(ik_x a_0/2\sqrt{3}) + 2\exp(-ik_x a_0/2\sqrt{3})\cos(k_y/2)$ for $\vec{k} = (k_x, k_y)$; $\Gamma = 2\cos(k_z c_0)$. The SWMcC model provides a treatment of the electron energy band near the Fermi level of graphite according to the $(k \cdot p)$ method based on the crystal symmetry. Parameters $\left(\gamma_0', \gamma_1', \gamma_2', \gamma_3', \gamma_4', \gamma_5', \Delta'\right)$ in the SWMcC model can correspond to the tight-binding hopping parameters individually [4,21]. In this work, the band structure of graphite along ΓKM (AHL) direction was measured over an energy range 28–116 eV by using ARPES. The band dispersion of graphite around the K point for each incident photon energy was sketched correctly from the fitted results of energy distribution curves (EDCs) and momentum distribution curves (MDCs) in photoemission intensity mapping results. To find the tight-binding hopping parameters in graphite, the inner potential V_0 in ARPES results was determined from the period of band dispersion for two π bands in KHK direction. Then the band structure of graphite sketched with the tight-binding method was compared with the band structure determined from the ARPES results at photon energies 49.91 eV and 84.08 eV to extract a set of tight-binding parameters. The band dispersion at other photon energies and the constant energy mapping results simulated with the extracted parameters were compared with ARPES result to examine the precision of fitted results. The parameters in this SWMcC model are obtained from the correspondence relation between the two methods. Fig. 2(a) shows the band structure of graphite in plane along ΓKM directions. We used reported SWMcC parameters [4] $E_0' = -0.024$ eV, $\gamma_0' = 3.16$ eV, $\gamma_1' = 0.39$ eV, $\gamma_2' = -0.02$ eV, $\gamma_3' = 0.315$ eV, $\gamma_4' = 0.044$ eV, $\gamma_5' = 0.038$ eV, $\Delta = -0.008$ eV in our calculations. The results are consistent with previous calculations [5,20]. Fig. 2(b) is an enlarged plot of Fig. 2(a) near the K point. Two touching points along the ΓKM direction are shown in Fig. 2(b): one is located in the $K\Gamma$ direction and another at the K point. Around the K point, there are four touching points between the valence and conduction bands. Three touching points are located at 0°, 120° and 240° deviating from the $K\Gamma$ line; a fourth point is located at the K point. A clear trigonal warping effect is visible in the contours of constant energy at the K point. Fig. 2(c) displays the simulated result of band dispersion along the KH direction. The π bands are most separated at the K point, but almost merge at the H point. Fig. 2(d) and (e) shows the simulated constant energy contours in plane at H ($k_z = 0.47$ Å^{-1}) and K ($k_z = 0$ Å^{-1}), respectively. Each contour separated by 0.1 eV is plotted from 0.1 eV to 0.7 eV in both pictures. A strong trigonal warping effect at the K point is visible. Because the trigonal warping effect is strongly affected by the value of γ_3, a larger $\gamma_3 = 0.443$ eV suggested recently from the de Haas–van Alphen effect implies that there exists a trigonal warping effect stronger than that proposed by preceding authors [9]. Fig. 2(f) shows contours of constant energy at 0.1, 0.5, 1.0 and 1.5 eV at the K point simulated with two proposed parameters of the SWMcC model; the set of parameters in solid blue lines is currently used in Fig. 2(a), and another contour set labeled with solid red lines uses the recently reported parameters

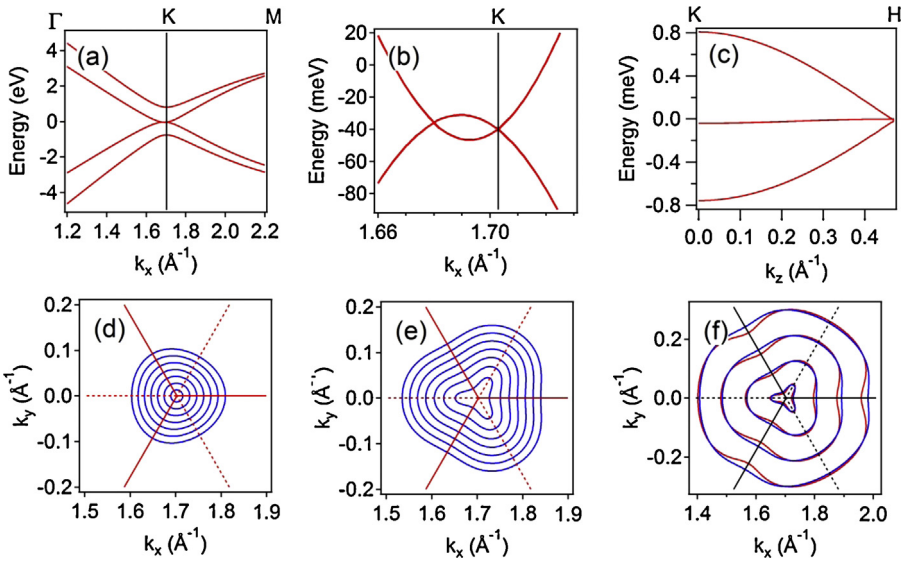

Fig. 2. (a) The band structure of graphite along the ΓKM direction; (b) enlarged band structure of (a) around the K point; (c) band dispersion along the KH direction; (d) constant energy contours at the H point; (e) constant energy contours at the K point; (f) comparison of constant energy contours with two reported parameters.

from the de Haas–van Alphen effect [9]. The difference in constant energy contours plotted with SWMcC parameters in Fig. 2(f) in two sets becomes larger at large binding energy, indicating that γ_3 can be evaluated correctly with a constant energy mapping result at large binding energies. To determine the tight-binding parameters, the constant energy mapping images were plotted from ARPES results to extract the tight-binding parameters correctly.

Because the intensity of ARPES is governed by the matrix element effect, we simulated this effect to plot correctly the constant energy mapping images and to compare with experimental results. The intensity of ARPES is governed by the product of a matrix element squared and a spectral function [22], $I(k, E_{kin}) \propto \left|M_{f,i}^{k}\right|^2 A(k, \omega)$. The matrix element term $M_{f,i}^{k}$ is defined by $\Psi_f(\vec{k}_f)|H_{\text{int}}|\Psi_i(\vec{k}_i)$, in which $\Psi_f(\vec{k}_f)$, $\Psi_i(\vec{k}_i)$ are wave functions of the final and initial states, respectively. Assuming the interaction term H_{int} to be treated in a dipole approximation $\left(\vec{A}\cdot\vec{p}\right)$ and the final state $\Psi_f(\vec{k}_f)$ considered to be a plane wave, the matrix element is expressed as [23]

$$M_{f,i}^{k} \propto \left(\vec{k}_f \cdot \vec{\varepsilon}\right) \int d^3\vec{r} e^{-i\vec{k}_f\cdot\vec{r}} \Psi_i\left(\vec{k}\right)$$

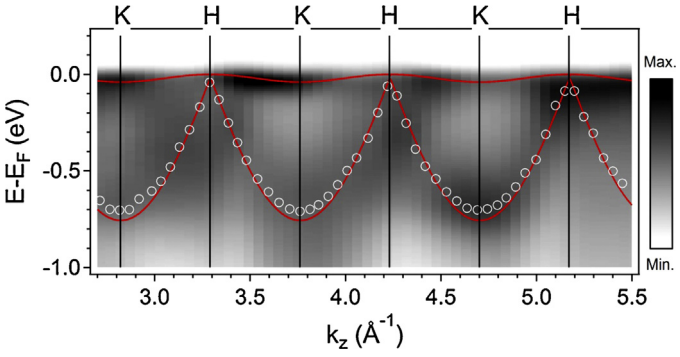

Fig. 3. Photoemission spectra in the KH direction with varied incident photon energies, where the incident photon energies are transformed to $k_\perp$ with chosen inner potential 17.25 ± 0.48 eV. The fitted peak positions of inner π band with varied $k_\perp$ values are labeled with white circles and the red lines are the simulated results of band dispersion along KH direction.

in which $\vec{k}_f$ is the momentum of the final state inside the solid, and $\vec{\varepsilon}$ is the polarization unit vector. Wave vector $\vec{k}_f$ is expressed as $\vec{k}_f = \vec{k}_{fz} + \vec{k}_{\parallel}$, in which wave vector k_{fz} is derived as the normal component of electron wave vector $k_\perp$. In ARPES experiments, the normal component of electron wave vector $k_\perp$ of the initial state

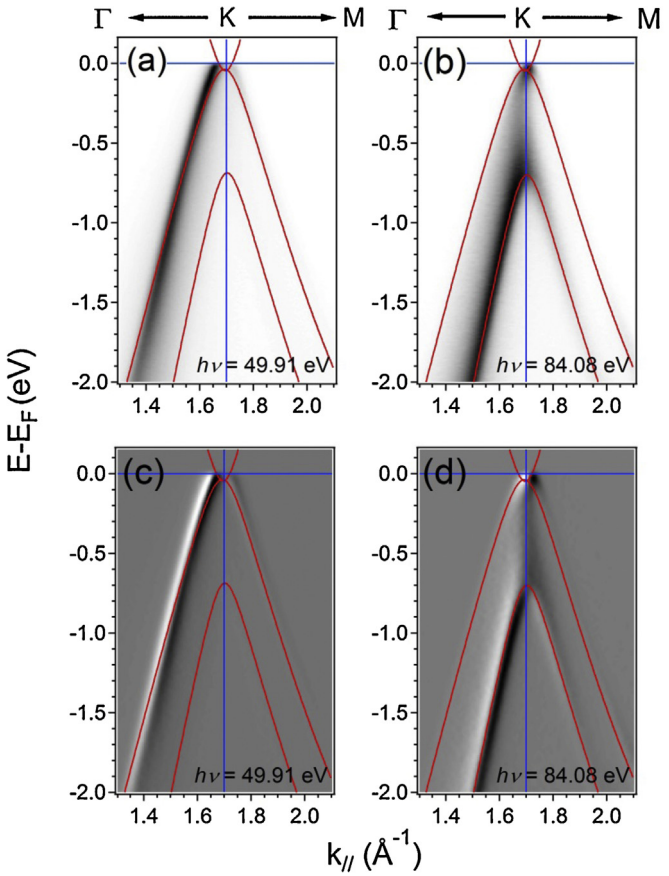

Fig. 4. False color plot of graphite EDC *vs* $k_{||}$ at photon energies 49.91 eV (a) and 84.08 eV (b). (c) and (d) are the first-derivative plots of (a) and (b). The solid lines are TB fits to data.

Table 1
SWMcC parameters (in eV) from the present and previous experimental works.

SWMcC parameters	Previous graphite[a]	Previous graphite[b]	Present work
γ_0'	3.16	3.15	3.12
γ_1'	0.39	0.375	0.355
γ_2'	−0.020	−0.0243	−0.020
γ_3'	0.315	0.443	0.24
γ_4'	0.044	0.07	0.12
γ_5'	0.038	0.05	0.038
Δ'	0.008	−0.002	−0.008
E_F	−0.024	−0.02505	−0.024

[a] Ref. [4].
[b] Ref. [9].

based on a free-electron model in the final state can be derived as [24]

$$k_\perp = \sqrt{\frac{2m}{\hbar^2}(E_{kin}\cos^2\theta + V_0)}$$

in which E_{kin} is the kinetic energy of the photoelectron, V_0 is the inner potential and θ is the angle between the emitted photoelectron and the detector. Because the intensity of photoemission is proportional to the interference term squared, a constant energy contour mapping image around the *K* point can be simulated from the product of the matrix element squared, the spectral function and a geometric factor including the polarization of the incident beam and the experimental geometry. The constant energy mapping images with the matrix element effect are simulated to compare with experimental data.

4. Results and discussion

Fig. 3(a) shows photoemission spectra in the *KH* direction with varied incident photon energy. At photon energy 28 eV ($k_z = 2.79\ \text{Å}^{-1}$) the peaks of two π bands are most separated. With increasing energy of the incident photon, the peak positions of two π bands merge gradually together, and separate again. The peak positions of the two π bands exhibit an oscillatory behavior with varied photon energy. The incident photon energy can be replaced with the normal component of electron wave vector $k_\perp$; a mapping image of the photoemission spectra along the *KH* direction over a wide energy range can be plotted as a function of $k_\perp$. The oscillation period of two π bands is π/c_0 in the image of photoemission intensities. The chosen inner potential V_0 is crucial and must satisfy a constraint that the period of two π bands merged together is equal to $n\pi/c_0$ with integer *n*. The fitted peak positions of inner π band with varied k_z values labeled with white circles and the simulated curves of dispersion in the *KH* direction are plotted in Fig. 3.

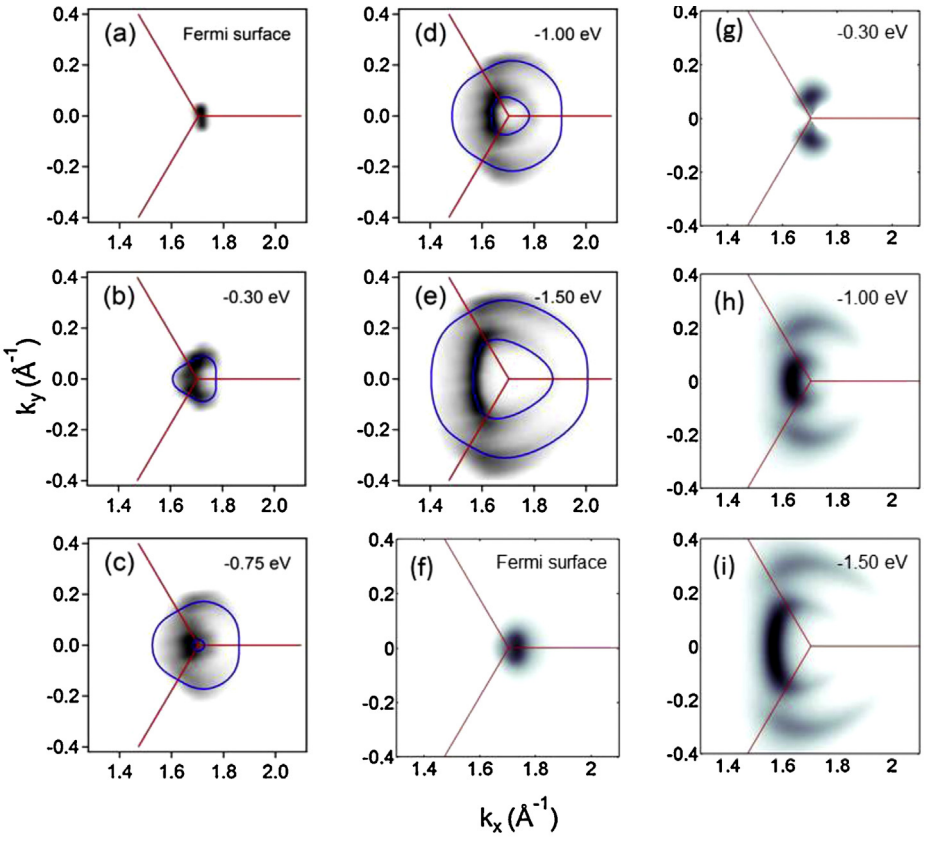

Fig. 5. (a–e) Results of constant energy mapping at the Fermi surface, −0.30, −0.75, 1.00 and 1.50 eV, respectively, of binding energy taken at photon energy 84.08 eV. (f–i) Simulated constant energy mapping images with the Fermi surface, −0.30, 1.00 and 1.50 eV, respectively.

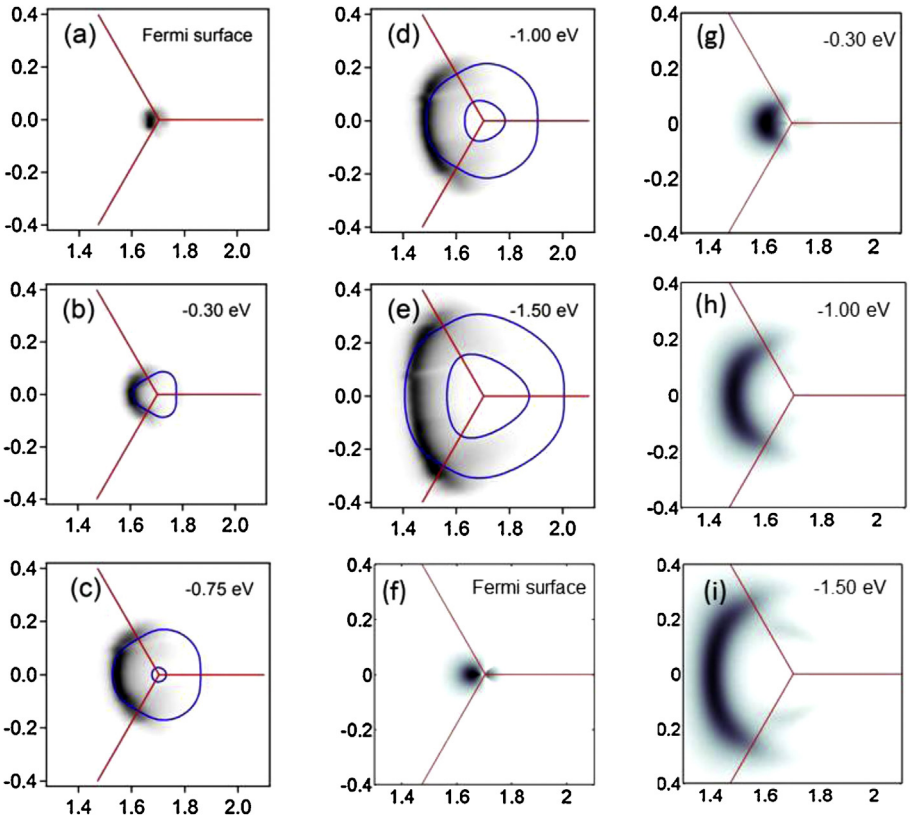

Fig. 6. (a–e) Results of the constant energy mapping at the Fermi surface, −0.30, −0.75, 1.00 and 1.50 eV, respectively, of binding energy taken at photon energy 49.91 eV. (f–i) Simulated constant energy mapping images with the Fermi surface, −0.30, 1.00 and 1.50 eV, respectively.

As shown in Fig. 3, the peak position of inner π band around the *H* point in experiments is extremely sensitive even with a few change of 0.025 Å^{-1} of k_z value, the behavior ensures the precision of the chosen inner potential because the variation of the inner potential also makes the change of k_z The inner potential $V_0 = 17.25 \pm 0.48$ eV for the present ARPES experiments is extracted with period π/c_0 from the band dispersion in the *KH* direction. The difference of peak positions for the inner π band at the *K* point between experimental result and simulation in Fig. 3 originates from a larger reported γ_1' value in the simulation [4].

Fig. 4(a) and (b) displays the band mapping results of photoemission intensity near the *K* point taken at photon energies 49.91 and 84.08 eV. The measured cut in Fig. 4(a) and (b) is along the *Γ*-*K*-*M* direction. The sharp band-mapping results allowed us to extract precisely the tight-binding parameters from the band dispersion of graphite. The photoemission intensity in the *KΓ* direction in Fig. 4 is strong for the momentum smaller than that at the *K* point, but rapidly decreases and vanishes in the *KM* direction for the momentum larger than that at the *K* point. Such behavior is attributed to the interference of wave functions of two π bands [23]. Fig. 4(c) and (d) shows the first derivative of the band-mapping results in Fig. 4(a) and (b), which are used to examine the fitted results of the tight-binding method. The bare band dispersion is governed mainly with the γ_0, γ_1, γ_3, γ_4 values; the slope of the band dispersion is governed by γ_0, the splitting energy of two π is mainly determined by γ_1 and the electron-hole asymmetry is originated from γ_4, but are insensitive to the change of the γ_2, γ_5 values. In contrast, the shape of the Fermi surface is more sensitive to the variation of the γ_2, γ_5 values.

In the present work, we use the reported γ_2, γ_5 values [4] and extracted other tight-binding parameters with results fitted from ARPES spectra. A comparison of present and previously proposed values is listed in Table 1. The calculated curves with extracted parameters are also overlapped on the experimental result in Fig. 4. Only a small deviation at photon energy 49.91 eV exists between the fitted curve and the experimental result at binding energy 2.0 eV. Our fitted result still shows satisfactory agreement with experimental data over a wide range of photon energy. A smaller extracted $\gamma_3 = 0.24$ eV from our extracted result implies a smaller trigonal warping existing in graphite, and is also near the value previously reported from the ARPES result [19,20].

We examine the accuracy of the extracted tight-binding parameters with constant energy contour plots; γ_3 is especially sensitive to the content of the trigonal warping effect in the constant energy mapping result. The simulated constant energy mapping images of the matrix element effect can be plotted and compared with experimental results.

Fig. 5(a)–(e) shows the results of the constant energy mapping at the Fermi surface, −0.30, −0.75, −1.00 and −1.50 eV, respectively, of binding energy taken at photon energy 84.08 eV. The incident beam has *p*-polarization in the dispersive plane. The fitted constant energy contours are also plotted in Fig. 5(a)–(e) and agree satisfactorily with experimental data. Fig. 5(f)–(i) displays the simulated constant energy mapping images with the Fermi surface, −0.30, 1.00 and 1.50 eV, respectively; a line of width 200 meV and Lorentzian shape is used in the spectral function. The simulated results are consistent with ARPES results. Fig. 6(a)–(e) shows the same results of the constant energy mapping at the Fermi surface, −0.30, −0.75, −1.00 and −1.50 eV, respectively, of binding energy taken at photon energy 49.91 eV. The experimental results in the *KM* directions in Fig. 6 exhibit a small deviation from the fitted constant energy contours at large binding energies, but the simulations of constant energy mapping images in Fig. 6(f)–(i) also duplicate the ARPES results, revealing the reliability of extracted tight-binding parameters in the present ARPES experiments.

5. Conclusions

We undertook high-resolution ARPES experiments on graphite samples of high quality over photon energies from 28 eV to 116 eV. The inner potential $V_0 = 17.25$ eV is determined with period $2\pi/c_0$ from the band dispersion in the *KH* direction. Parameters in the tight-binding method and SWMcC model in graphite are extracted from the fitted results of the ARPES experiments. A comparison of constant energy mapping results in both simulation and ARPES experiments at large binding energies confirms the reliability of the extracted tight-binding parameters.

Acknowledgments

The Ministry of Science and Technology of Taiwan provided support under grant: NSC 99-2112-M-213-006-MY3. NSRRC is operated under the Ministry of Science and Technology of Taiwan.

References

[1] P.R. Wallace, Phys. Rev. 71 (1947) 622.
[2] J.C. Slonzewski, P.R. Weiss, Phys. Rev. 109 (1958) 272.
[3] J.W. McClure, Phys. Rev. 108 (1957) 612.
[4] M.S. Dresselhaus, G. Dresselhaus, Adv. Phys. 51 (2002) 1.
[5] J.-C. Charlier, J.-P. Michenaud, X. Gonze, J.-P. Vigneron, Phys. Rev. B 44 (1991) 13237.
[6] J.-C. Charlier, J.-P. Michenaud, X. Gonze, Phys. Rev. B 46 (1992) 4531.
[7] S.J. Williamson, S. Foner, M.S. Dresselhaus, Phys. Rev. 140 (1965) A1429.
[8] S.B. Hubbard, T.J. Kershaw, A. Usher, A.K. Savchenko, A. Shytov, Phys. Rev. B 83 (2011) 035122.
[9] J.M. Schneider, B.A. Piot, I. Sheikin, D.K. Maude, Phys. Rev. Lett. 108 (2012) 117401.
[10] D.E. Soule, J.W. McClure, L.B. Smith, Phys. Rev. 134 (1964) A453.
[11] J.M. Schneider, M. Orlita, M. Potemski, D.K. Maude, Phys. Rev. Lett. 102 (2009) 166403.
[12] S.B. Hubbard, T.J. Kershaw, A. Usher, A.K. Savchenko, A. Shyto, Phys. Rev. B 83 (2011) 035122.
[13] R.E. Doezema, W.R. Datars, H. Schaber, A. Van Schyndel, Phys. Rev. B 19 (1979) 4224.
[14] A. Misu, E.E. Mendez, M.S. Dresselhaus, J. Phys. Soc. Jpn. 47 (1979) 199.
[15] W.W. Toy, M.S. Dresselhaus, G.D. Dresselhaus, Phys. Rev. B 15 (1977) 4077.
[16] M. Orlita, C. Faugeras, G. Martinez, D.K. Maude, M.L. Sadowski, M. Potemski, Phys. Rev. Lett. 100 (2008) 136403.
[17] D.E. Soule, Phys. Rev. 112 (1958) 698.
[18] L.-C. Tung, P. Cadden-Zimansky, J. Qi, Z. Jiang, D. Smirnov, Phys. Rev. B 84 (2011) 153405.
[19] A. Grüneis, C. Attaccalite, T. Pichler, V. Zabolotnyy, H. Shiozawa, S.L. Molodtsov, D. Inosov, A. Koitzsch, M. Knupfer, J. Schiessling, R. Follath, R. Weber, P. Rudolf, L. Wirtz, A. Rubio, Phys. Rev. Lett. 100 (2008) 037601.
[20] A. Grüneis, C. Attaccalite, L. Wirtz, H. Shiozawa, R. Saito, T. Pichler, A. Rubio, Phys. Rev. B 78 (2008) 205425.
[21] B. Partoens, F.M. Peeters, Phys. Rev. B 74 (2006) 075404.
[22] A. Damascelli, Z. Hussain, Z.X. Shen, Rev. Mod. Phys. 75 (2003) 473.
[23] E.L. Shirley, L.J. Terminello, A. Santoni, F.J. Himpsel, Phys. Rev. B 51 (1995) 13614.
[24] A. Damascelli, Phys. Scr. 2004 (2004) 61.